EUROfusion

WPMAT-PR(18) 20424

A. Puype et al.

Design of reduced activation ferritic-martensitic steels with improved creep resistance by thermodynamic modelling

Preprint of Paper to be submitted for publication in
Acta Materialia

This work has been carried out within the framework of the EUROfusion Consortium and has received funding from the Euratom research and training programme 2014-2018 under grant agreement No 633053. The views and opinions expressed herein do not necessarily reflect those of the European Commission.

Design of reduced activation ferritic-martensitic steels with improved creep resistance by thermodynamic modelling

A. Puype[1,2*], G. Bonny[2] and L. Malerba[2]

[1] Department of Electrical Energy, Metals, Mechanical Constructions and Systems, Ghent University, Technologiepark 903, B-9052 Zwijnaarde, Belgium.
[2] Nuclear Materials Science Institute, SCK·CEN, Boeretang 200,B-2400 Mol, Belgium.

Abstract

An approach based on the systematic use of thermodynamic modelling has been worked out and applied for the development of reduced activation ferritic/martensitic (RAFM) steels with improved creep resistance by composition tuning. Initially, a series of Thermo-Calc® calculations were performed to construct a database of phase equilibria. Based on this database and constraints deduced from literature, compositions with potentially better creep resistance were identified. The model was then fine-tuned by adding new constraints to find compositions and accompanying heat treatments that should result in the anticipated improved mechanical properties. An experimental heat resembling an optimized alloy according to the model was characterized and found to show improved creep resistance compared to the reference steel, EU97-2, thereby validating the model.

KEYWORDS Reduced activation steels, thermodynamic modelling, creep, Thermo-Calc, experimental steel

1. Introduction

Reduced activation ferritic/martensitic (RAFM) steels are considered as candidate structural materials for fusion reactors because of their good swelling resistance, low thermal expansion and high thermal conductivity [1]. The European variant of a RAFM steel is EUROFER97 (EU97). The composition of EU97 [2] was obtained by replacing high activation alloying elements typically found in commercial 9Cr-1Mo steels, like T91 [3] with lower activation ones, for easier waste disposal. Specifically, the high activation elements Mo, Nb, Ni and Co, were replaced with equivalent concentrations of W, Ta and V.

Table 1: Chemical compositions of T91, EU97 and experimental grade 0.05C_0.037N. The Fe content is given by the balance.

[wt%]	C	Mn	Si	Cr	Mo	W	N	V	Ta	B	Al	Ni
T91	0.08-0.12	0.3-0.6	0.2-0.5	8.0-9.5	0.85-1.05	-	0.03-0.0.7	0.18-0.25	-	-	<0.4	<0.4
EU97	0.09-0.12	0.2-0.6	0.05	8.5-9.5	-	1.0-1.2	0.015-0.045	0.15-0.25	0.10-0.14	-	-	-
0.05C_0.037N	0.049	0.44	0.04	8.8	-	0.98	0.037	0.28	0.19	0.0065	-	-

The existing RAFM grades are designed for first wall structural steels with an optimal service temperature in the window of 350 - 550°C [4], limiting the allowable interface temperature to about 550 °C. Higher operating temperatures are, however, targeted for increased operation capabilities at which the RAFM steels currently exhibit inacceptable loss of strength due to creep [5, 6].

The creep resistance of ferritic/martensitic steels can be improved by effective obstruction of sub-yield dislocation motion by introducing fine stable MX (M = V and/or Ta, X = C or N) carbonitrides in the martensitic matrix [7, 8], as well as increasing the solid solution alloying [9] and decreasing the grain size [10]. The time to rupture can be increased by suppressing grain boundary sliding and avoiding the presence of large particles at the grain boundaries. Thus, the material must have a tempered martensitic matrix with fine uniformly distributed MX and a limited fraction of large $M_{23}C_6$ carbides on the grain boundaries. This type of microstructure is typically obtained by a normalization, quench and temper treatment. During normalization, $M_{23}C_6$ and MX precipitates dissolve completely or partially in the austenitic matrix, respectively, depending on temperature. The final grain size of the material also depends on the normalization temperature, as well as on the holding time before quenching. During the tempering step, the $M_{23}C_6$ and MX will reprecipitate with a finer size distribution and the martensite will soften, so part of the material's toughness is retrieved. The parameters of the heat treatment and the alloying elements are therefore directly related to the final mechanical properties of the material and can therefore be optimized.

Nowadays, it has become customary to use thermodynamic packages such as Thermo-Calc® as a guide to check the influence of composition and temperature, often chosen based on experience or intuitive criteria, on the range of stability of phases at thermodynamic equilibrium. The thermodynamic (TD) modelling approach proposed here goes beyond the classical use of thermodynamic packages. It is based on the idea of manipulating a large database, obtained by a systematic and intensive use of Thermo-Calc® in a broad range of compositions and temperatures, to identify the optimal steel composition and heat treatment temperatures for the optimization of the creep resistance. The criteria behind the optimization take their origin from the known fact that mechanical degradation after long-term exposure at high temperature stems from the coarsening of precipitates and the extended recovery of the martensitic structure [4, 5]. The search algorithm finds the optimum conditions via suitable criteria to identify a subset of compositions and temperatures (both normalization

temperature, T_{norm}, and tempering temperature, T_{temp}). The optimization criteria are then refined, or different sets of criteria are considered, until convergence to a specific optimal composition and heat treatment parameters is obtained. Eventually, a steel with a composition and heat treatment parameters close to the optimum found from the TD model was identified amongst a set of already manufactured steels. Mechanical tests were performed to verify that the DBTT and yield strength is similar to the reference material, while the creep resistance is improved, thereby allowing the validity of the TD modelling approach to be experimentally verified.

2. Methods

2.1. Experimental techniques

The composition of EU97 is given in Table 1, as a reference for the ranges of alloying elements used in the thermodynamic calculations. Additionally, the composition of the experimental reduced activation ferritic/martensitic (RAFM) heat used to validate the model is also shown in Table 1. The latter is denoted as 0.05C_0.037N.

The cast of the 0.05C_0.037N grade was thermo-mechanically (TM) treated according to the procedure described in [12]. The TM treatment implied the rolling of the cast in six consecutive rolling passes at a predefined fixed temperature to a final thickness of 11 mm at a final rolling temperature of 850 °C. After the TM treatment, the material was annealed at a normalization temperature (T_{norm}) of 1050 °C for 30 minutes followed by water quenching. The plate was subsequently tempered at a tempering temperature (T_{temp}) of 750 °C for 2 hours, and then air cooled. The critical temperatures for the 0.05C_0.037N grade were determined by dilatometry. T_{norm} was chosen as A_{c3} + 100 °C, the tempering temperature on the other hand was chosen by analogy with to the tempering treatment of EU97-2 [2].

The microstructural characterization was performed using light optical microscopy (LOM), electron back scattered diffraction (EBSD) and scanning transmission electron microscopy (STEM). The precipitates were analyzed by electron diffraction spectrometry (EDS) and inductively coupled plasma mass spectrometry (ICPMS). The STEM images were post-analyzed by ImageJ to determine the size of the precipitates [12].

The tensile tests were carried out in a 250 kN load-capacity Zwick Z250 machine following NBN EN ISO 6892-1 standard on A50 specimens with L-orientation [13].

Specimens with L-T orientation according to ISO 148-1, were tested on a 750 J Charpy test unit at temperatures ranging between -150°C and 50 °C. The data was fitted with $E = (LSE + D/2) + D/2 \times \tanh$ ¿, with $D = USE - LSE$, C = slope of transition region and T_0 = ductile-to-brittle transition temperature (DBTT) [13].

Creep tests on specimens with L-orientation were performed under air using a lever arm creep machine following European standard NF ISO 204 from August 2009. The creep specimens have a 40 mm full length and a diameter of 4 mm. The stress controlled tests were carried out at 650°C with stresses of 170 MPa and 100 MPa.

2.2. Thermodynamic model

Thermodynamic equilibrium calculations were performed using the Thermo-Calc® 2017a software [14] in combination with the thermodynamic database TCFE7: Steels/Fe-Alloys v7.0 [15]. The latter is designed to describe the thermodynamics of high-Cr ferritic-martensitic steels. The output of the thermodynamic calculations is the equilibrium volume fraction (f_{vol}) of the different equilibrium phases at a given temperature, pressure and composition.

Thermo-Calc® calculations were systematically performed in the range of temperature and compositions given in Table 2 (the pressure was constant and set to the atmospheric value, 101.3 kPa), on an equidistant grid consisting of 11 points on the T axis and 6 points on the C_X axis. T_{norm} ranged between 900 - 1150 °C, while 650-780 °C serves as the range for T_{temp}. This scheme resulted in $11 \times 6^6 = 513{,}216$ equilibrium calculations, requiring a total of ~720 CPU hours. As a result, f_{vol} was obtained on each grid point for the following phases: ferrite solid solution, austenite solid solution, $M_{26}C_6/M_3C_2/M_5C_2/M_6C/M_7C_3$ carbides, VN and TaC carbonitrides. Values between grid points were determined via multi-linear interpolation.

Table 2: The temperature range, pressure and composition range explored in the thermodynamic calculations.

T [°C]	p [kPa]	C_{Si} [wt.%]	C_{Mn} [wt.%]	C_C [wt.%]
650 – 1150	101.30	0.03	0.4	0.02 – 0.15
C_{Cr} [wt.%]	**C_N [wt.%]**	**C_V [wt.%]**	**C_{Ta} [wt.%]**	**C_W [wt.%]**
8.5 – 9.8	0.03 – 0.07	0.15 – 0.5	0.15 – 0.5	0.5 – 2.5

By scanning and treating the output of the calculation as a function of T_{norm}, T_{temp}, and the different concentrations (C_X with X = C, Cr, N, V, Ta and W), f_{vol} maxima for vanadium nitrides (VN) and tantalum carbides (TaC) were obtained under given constraints based on metallurgical arguments (see section 3.1). The physical problem corresponds to a numerical constrained optimization in 8 dimensions. The interpolation allowed the local optima to be identified; the optimum of all local optima provided the global optimum.

3. Results

3.1. Thermodynamic model

Table 2 shows the investigated composition ranges, which were fairly wide in comparison with the EU97 composition (Table 1). The Cr content was centered around 9 wt% Cr because this composition provides an optimum in terms of minimum DBTT shift after irradiation [16]. However, it is considered that a moderate variation of Cr content may help improving the microstructure in terms of creep strength, without significantly increasing the DBTT shift. The reasons for changing the content of the other elements are plenty and, depending on the criteria, an increase or decrease of the same element may be suggested, making a numerical optimization based on thermodynamic indications highly desirable. The content of V, Ta, C and N should be increased to maximize the fraction of MX (M= V and/or Ta and X= C or N). However, the C content is allowed to be as low as 0.02 wt%, to study the possibility of having

very low carbon RAFM steels, given that this could be beneficial to mitigate irradiation embrittlement. As a matter of fact, less carbon in the material is expected to reduce the formation of dislocation loops and vacancy clusters under irradiation, thereby mitigating the irradiation hardening that is a source of embrittlement [17]. The W content was extended in the optimization process to allow for the contribution of W in the formed phases. The Z-phase, however, was suspended from the calculations, as it is considered to be an equilibrium phase that only occurs in 9 wt% Cr steels after extended exposure to high temperature [18]. Moreover, thermodynamic calculations show that no Laves phase is formed in the considered 9 wt% Cr steels at 650 °C, so this phase is suspended from the calculations as well.

The algorithm searches for the compositions with the highest f_{vol} of MX carbonitrides and a zero f_{vol} of M_xC_y ($M_{23}C_6$, M_3C_2, M_5C_2, M_6C and M_7C_3) carbides at T_{temp}, in a fully martensitic matrix (a complete martensitic structure is ensured by imposing that the ferrite fraction is zero at T_{norm}). MX carbonitrides are indeed preferred in the matrix over $M_{23}C_6$ carbides due to their very low coarsening rate and their contribution to the strength of the material [19]. The maximization of the MX f_{vol} is performed first without any constraints added (Table 3), and then after adding, one by one, three constraints, namely: $T_{norm} \leq 1050$ °C ("T_norm_limit"); $C_C > 0.02$ wt% C ("C_limit") and, finally, f_{vol} of VN minimal at T_{norm} ("VN_min"). Adding a constraint to the algorithm creates a subset of the thermodynamic database in which the maximum f_{vol} of MX is searched. Adding more constraints further refines the subset, limiting the number of compositions in which the MX fraction can be maximized.

Table 3: The constraints and conditions considered in the search algorithm.

Constraints	Conditions for type MX
Unconstrained ("Unconstrained")	**VN_{MAX} (only the f_{vol} of this type of MX is maximized)**
Impose upper limit to T_{norm} ("T_norm_limit"): keep PAG size small	**MIX (a 50/50 % f_{vol} is maximized)**
Lower limit C_C ("C_limit"): guarantee sufficient amount of C to produce martensite	**TaC_{MAX} (only the f_{vol} of this type of MX is maximized)**
Minimum f_{vol} VN at T_{norm} ("VN_min"): guarantee reprecipitation of small size VN	

The first constraint limits T_{norm} to $T_{norm} \leq 1050$ °C in order to avoid extensive austenitic grain growth (Table 3). The constraint is based on experimental results found in literature [2, 17]. The data presented by K.S. Chandravathi et al. [21] shows an exponential increase of prior austenite grain size (PAGS) depending on T_{norm}, with a sharp change in growth rate around 1050 °C (Fig. 3 in [21]). The strong dependence of grain growth with normalization temperature resembles the results for RAFM experimental EUROFER steel published by Puype *et. al.* (Fig. 3 in [12]), thus the choice of this temperature seems warranted. The second constraint that was added imposes a lower limit on the carbon content (Table 3). The reason for this constraint is that it was experimentally shown that, if the carbon content is too low, ferrite formation during quenching is inevitable [13,22,23]. The last additional constraint corresponds to minimizing the calculated fraction of VN at the chosen normalization temperature (Table 3). This criterion is suggested based on the consideration that, to further improve the creep resistance of the steel, the VN precipitates should be as finely dispersed as

possible. If VN is minimized at T_{norm}, most of the VN precipitates dissolve during normalization, so the VN nitrides can reprecipitate in a finer and more homogeneous fashion during tempering. The latter is preferred compared to having a coarsening of the precipitates that nucleated during normalization. This condition can only be applied to VN nitrides as the dissolution temperature of TaC is too high and would lead to extensive austenitic grain growth. Additionally, it was verified that it is beneficial that f_{vol} of TaC be non-zero at T_{norm}, to pin grain boundaries and further limit prior austenite grain growth [24].

The optimal concentrations of C_X will vary depending on the type of MX that is maximized: the focus can be on vanadium carbonitrides only, tantalum carbides only, or equal weight to both. Three distinct conditions were therefore explored (Table 3), i.e., 100% weight on the VN fraction (VN_{MAX}), 100% weight on the TaC fraction (TaC_{MAX}), or a 50/50% mixture of both MX carbonitrides fractions (*MIX*). The results for C_X (X = C, V, N and Ta) and T_{norm} are summarized in Fig. 1 and Fig. 2, respectively, as they will depend on either the type of condition or the imposed constraints. C_W, C_{Cr} and T_{temp}, in contrast, are independent of the conditions and will not vary when introducing additional constraints. These values, determined in the "unconstrained" condition, are C_W = 0.5 wt%, C_{Cr} = 8.9 wt% and T_{temp} = 780°C. These values are excluded from Fig. 1 and Fig. 2, respectively, for clarity.

Different local optima for C_X are found by the algorithm in unconstrained state and after applying all the constraints (Fig. 1). The optimal C_C and C_{Ta} is either 0.02 wt% C or 0.046 wt % C and 0.15 wt% Ta or 0.50 wt% Ta, respectively. For C_V and C_N the optima are 0.5 wt% V or 0.36 wt% V and 0.07 wt% N and 0.03 wt% N, respectively. If the condition TaC_{MAX} is considered, so maximizing the f_{vol} of TaC, the C_C and C_{Ta} present in the material will need to be high and the C_V and C_N will need to be low and vice versa in the case of condition VN_{MAX}. For TaC_{MAX}, the algorithm therefore selects C_C = 0.046 wt%, C_{Ta} = 0.5 wt%, C_V = 0.36 wt% and C_N = 0.07 wt%, as these are the highest values for the optima of C_C and C_{Ta} and the lowest values for the optima of C_V and C_N (Fig. 1 (c)). The main difference between TaC_{MAX} and VN_{MAX} is that the C_X values in the TaC_{MAX} condition are independent of the applied constraints (Fig. 1 (c)). Therefore, the following discussion on the variation of the C_X with the constraints will focus on the VN_{MAX} condition only. The variation of the optimal C_V and C_N with the constraints is similar in the VN_{MAX} and *MIX* conditions (Fig. 1 (a) & (b)), as is the variation of C_{Ta} and C_C with the constraints in *MIX* and TaC_{MAX} conditions (Fig. 1 (b) & (c)).

The initial simulated composition for the VN_{MAX} condition, with no constraints added, is an alloy with 0.02 wt% C, 0.15 wt% Ta, 0.07 wt% N and 0.05 wt% V (Fig. 1 "Unconstrained"). The C_V and C_N are at the upper limit and C_C and C_{Ta} are at the lower limit of the allowable range (Table 2). These values for C_X don't change when the normalization temperature criterion is added to the search algorithm (Fig. 1 "T_norm_limit").

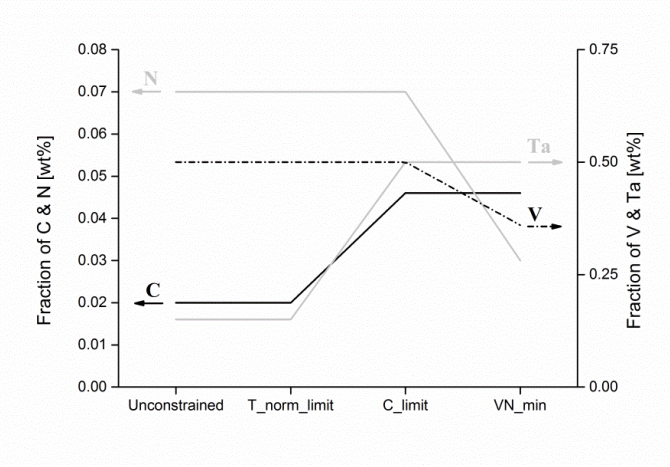

(a)

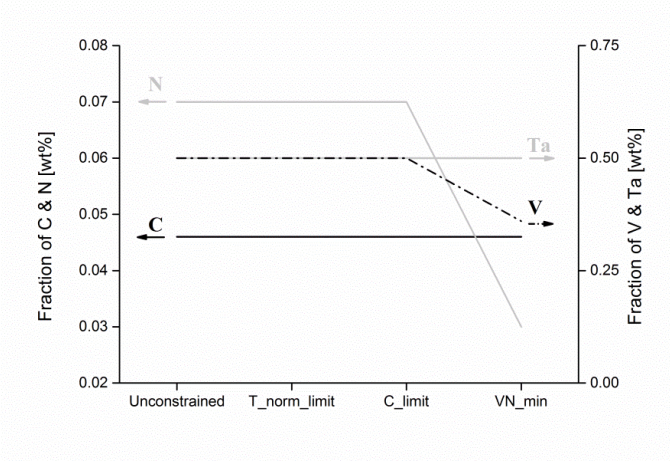

(b)

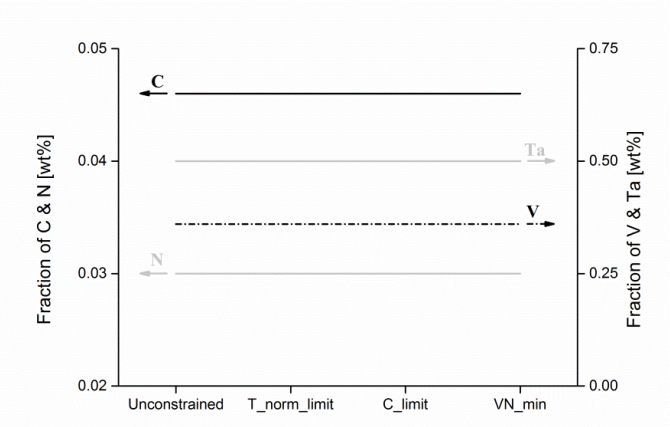

(c)

Fig. 1: Optimal concentrations of C, N, V and Ta to maximize the f_{vol} of MX for conditions (a) VN_{MAX} ,(b) *MIX* and (c) TaC_{MAX} after imposing the additional constraint: 1) no additional constraint ("Unconstrained"); 2) $T_{norm} \leq 1050$ °C ("T_norm_limit") ; 3) $C_C > 0.02$ wt% ("C_limit") and 4) f_{vol} VN minimal at T_{norm} ("VN_min").

When imposing a lower limit on the carbon content, the optimal C_C and C_{Ta} change and increase from 0.02 wt% to 0.046 wt% and from 0.15 wt% to 0.5 wt%, respectively (Fig. 1 (a) "T_norm_limit" vs. "C_limit"). However, increasing the threshold of carbon further rendered no different optimum.

Additionally, the VN minimization constraint affects T_{norm}, as well as the optimal C_V and C_N. The C_N decreased from 0.07 to 0.03 wt%, C_V decreases from 0.5 wt% to 0.36 wt% and T_{norm} increases from 900 °C to 1050 °C (Fig. 1 "C_limit" vs. "VN_min").

When no additional constraint is imposed (Fig. 2 "Unconstrained"), the search algorithm reveals that, independently of the MX condition, a temperature range of T_{norm} between 900 °C and 1150 °C and T_{temp} of 780 °C, should be considered in order to have the highest f_{vol} of MX carbonitrides during tempering. The normalization temperature criterion obviously has an effect on T_{norm}, which decreases from 1150 °C to 1050 °C (Fig. 2 "T_norm_limit). The minimization of VN f_{vol} at T_{norm} increases the lower limit of the T_{norm} range to 1050 °C (Fig. 2 "VN_min"). The optimal heat treatment with the used constraints is therefore T_{norm} = 1050 °C and T_{temp} = 780 °C.

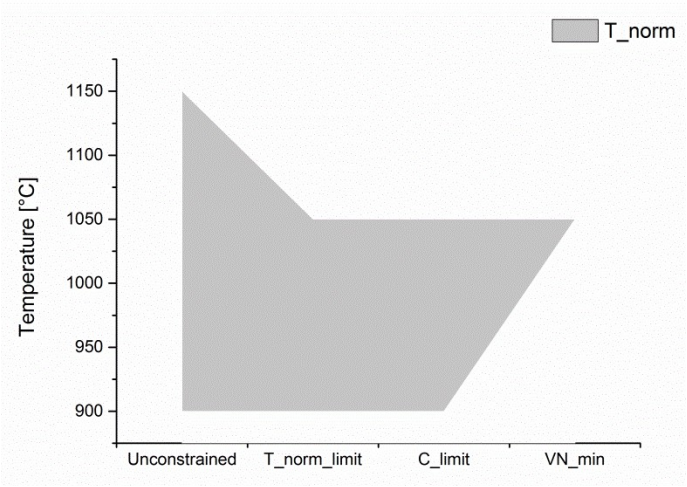

Fig. 2: Normalization temperature range for all conditions after imposing the additional constraint: 1) no additional constraint ("Unconstrained"); 2) $T_{norm} \leq$ 1050 °C ("T_norm_limit") ; 3) $C_C >$ 0.02 wt% ("C_limit") and 4) f_{vol} VN minimal at T_{norm} ("VN_min").

After all the applied constraints, the model gives a fixed T_{norm} of 1050 °C, where the composition, consisting of 0.046 wt% C, 8.9 wt% Cr, 0.5 wt% W, 0.03 wt% N, 0.36 wt% V and 0.5 wt% Ta, contains a maximum f_{vol} of fine MX precipitates that form during tempering, which is expected to lead to an improved creep response in comparison with EU97-2.

Other compositions are proposed at different T_{temp}, which could also lead to improved creep properties. The compositions that have maximum MX precipitation after normalization at 1050 °C as a function of tempering temperature are given in Table 4.

Table 4: Compositions with varying tempering temperature which have maximum MX precipitation at T_{temp} after normalization at 1050 °C.

	T_{norm} [°C]	T_{temp} [°C]	C_C [wt%]	C_{Cr} [wt%]	C_N [wt%]	C_V [wt%]	C_{Ta} [wt%]	C_W [wt%]
1.	1050	780	0.046	8.9	0.03	0.36	0.5	0.5
2.	1050	770	0.046	8.9	0.03	0.43	0.5	0.5
3.	1050	760	0.046	8.9	0.03	0.43	0.5	0.5
4.	1050	750	0.046	8.9	0.03	0.43	0.5	0.5
5.	1050	740	0.046	8.9	0.03	0.43	0.5	0.5

6.	1050	730	0.046	8.9	0.03	0.43	0.5	0.5
7.	1050	720	0.046	8.5	0.03	0.5	0.5	0.5
8.	1050	710	0.046	8.5	0.03	0.5	0.5	0.5
9.	1050	700	0.046	8.5	0.03	0.5	0.5	0.5
10.	1050	690	0.046	8.5	0.03	0.5	0.5	0.5
11.	1050	680	0.046	8.5	0.03	0.5	0.5	0.5
12.	1050	650	0.046	8.7	0.07	0.22	0.36	0.9

Table 4 shows that, with increasing V, the tempering temperature suggested as optimal by the algorithm decreases, except for the composition 0.046 wt% C, 8.7 wt% Cr, 0.07 wt% N, 0.22 wt% V, 0.36 wt% Ta and 0.9 wt% W. This is the only composition (Table 4 nr. 12) that differs from the others in C_N, C_{Ta} and C_W. It is thus an interesting alloy, even though it does not render the maximum theoretically obtainable of MX precipitation at T_{temp}, as can be seen in Fig. 3. The composition nr. 12, tempered at 650 °C, will render the same volume fraction of VN at tempering temperature as the other listed compositions, but the volume fraction of TaC at T_{temp} will be significantly less. The composition nr. 12 gives in fact the lowest volume fraction of TaC at T_{norm} and is therefore the other extreme to our optimal composition (Table 4 nr. 1) where we looked for the composition with a minimum volume fraction of VN at T_{norm}.

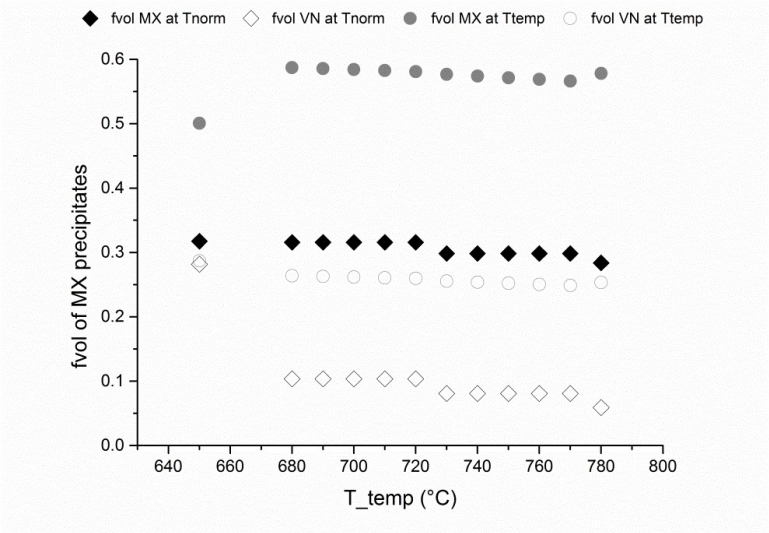

Fig. 3: Volume fraction of total MX precipitates and VN precipitates at normalization and tempering temperature with T_{norm} = 1050 °C.

3.2. Experimental heat

The compositions of the alloy nr. 12 suggested by the model with heat treatment of T_{norm} = 1050 °C and T_{temp} = 650 °C, the experimental heat 0.05C_0.037N and EU97-2 are compared in Table 5.

Table 5: Compositions of EU97-2, 0.05C_0.037N and simulated alloy nr. 12 (Table 4 nr. 12).

T [°C] / X [wt%]	T_{norm}	T_{temp}	C	Mn	Si	Cr	W	N	B	V	Ta	Fe
EU97-2	980	750	0.11	0.53	0.050	8.8	1.1	0.040	-	0.20	0.12	Bal.
0.05C_0.037N	1050	750	0.049	0.44	0.040	8.8	0.98	0.037	0.0065	0.28	0.19	Bal.
Alloy nr. 12	1050	650	0.046	0.40	0.030	8.7	0.90	0.070	-	0.22	0.36	Bal.

The quench and tempering (Q&T) treatment of the experimental alloy 0.05C_0.037N was treated at a similar T_{norm} as the simulated T_{norm} = 1050 °C of alloy nr. 12, although the T_{temp} was higher (T_{temp} = 750 °C instead of 650 °C, see Table 5).

The optical micrograph of 0.05C_0.037N after Q&T treatment is given in Fig. 4. The optical micrograph of EU97-2 is added for comparison.

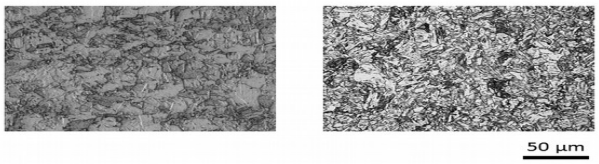

Fig. 4: Optical micrograph of 0.05C_0.037N grade (left), etched with Vilella's etchant and LOM image of EU97-2 [2] **(right), for comparison.**

OIM analysis of EBSD data was used to quantify the block size and PAGS of the 0.05C_0.037N grade. Fig. 5 shows the image quality (IQ) map of 0.05C_0.37N, in which the high angle grain boundaries (HAGB) are indicated by black lines. The martensitic blocks were determined as grains confined by HAGB, having a misorientation above or equal to 15°. With this boundary condition, the equivalent block diameter was determined as 7.0 ± 1.0 µm. A linear intercept method was used on the grain boundaries, with a misorientation between 21.1° and 47.1° to determine the PAGS, as described by Bernier [25]. The average size of the PAG is 12.0 ± 1.1 µm. For comparison, the average martensitic grain size (GS) of EU97-2 is 10 µm [2] after Q&T treatment with T_{norm} = 980 °C and T_{temp} = 760 °C.

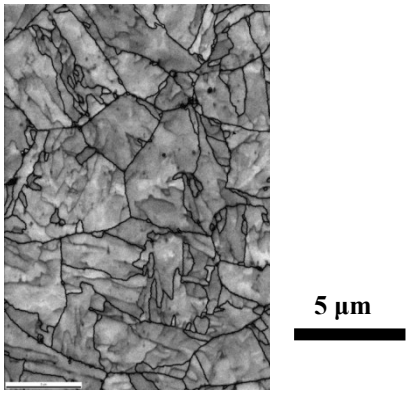

Fig. 5: Image quality (IQ) map of 0.05C_0.037N grade with high angle grain boundaries (HAGB) indicated with black lines.

The combined techniques ICPMS, STEM and EDS were used to determine the size distribution of the precipitates (Fig. 6). The average equivalent diameter of MX carbonitrides is 28 ± 1 nm and the average equivalent diameter of $M_{23}C_6$ carbides is 172 ± 9 nm. ICPMS data from the 0.05C_0.037N grade showed that the alloying elements, V, Ta, W and Cr remained mostly in solid solution after Q&T. Only, 39 % and 49 % of the V and Ta bulk concentration precipitated, respectively, and roughly 5 % of either W and Cr content.

(a)

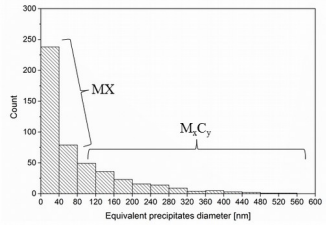

(b)

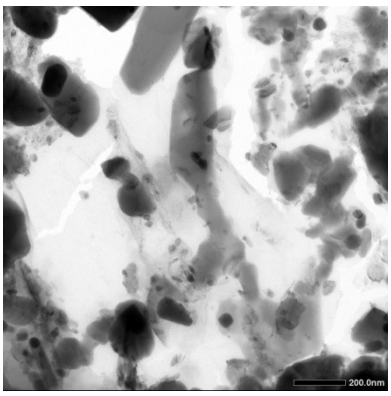

Fig. 6: (a) Size distribution of MX and $M_{23}C_6$ precipitates found in 0.05C_0.037N and (b) STEM image of 0.05C_0.037N.

The hardness, tensile and impact properties of the 0.05C_0.037N grade in comparison with EU97-2 [2] are given in Table 6 and show that the experimental alloy has equivalent basic mechanical properties to the reference steel EU97-2.

Table 6: Tensile and impact data for 0.05C_0.037N grade in comparison with EU97-2.

Steel grade	DBTT [°C]	USE [J]	HV [HV5]	YS [MPa]	UTS [MPa]
EU97-2	-40	270	219	543	683
0.05C_0.037N	-51 ± 3	197 ± 3	223 ± 1	593 ± 2	694 ± 2

Creep experiments were performed on 0.05C_0.037N at 650 °C with a stress of 100 MPa. Within 3750 hr. no rupture occurred. In contrast, the time to rupture for plates of EU97-2 tested at 650 °C with a stress of 100 MPa is less than 500 hr. [2] (Fig. 7).

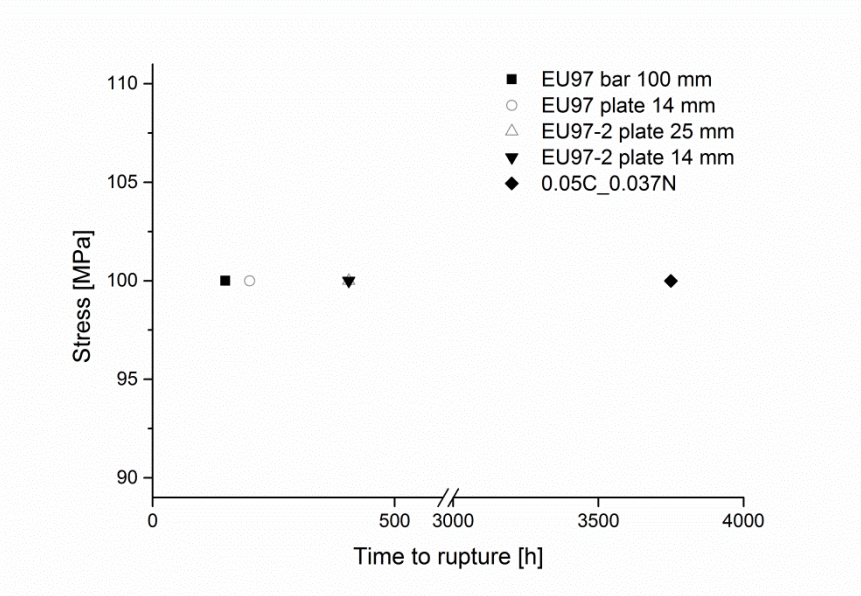

Fig. 7: Time to rupture of EU97 round bar, EU97 plate of 14 mm, EU97-2 plate of 25 mm, EU97-2 plate of 14 mm (data from [2]) and experimental grade 0.05C_0.037N for creep tests at 650 °C and 100 MPa.

4. Discussion

The reduced activation ferritic/martensitic (RAFM) steels obtain their functional properties by a two-stage heat treatment, which consist of an annealing stage followed by quenching and an additional tempering stage. This thermal treatment creates a microstructure of tempered martensite with precipitates. EU97-2, in particular, comprises of two main types of precipitates, i.e., the MX carbonitrides and $M_{23}C_6$ carbides. The carbonitrides are stable precipitates with a typical size between 20-60 nm. The $M_{23}C_6$ carbides, on the other hand, whose average size is between 80-200 nm [20], tend to coarsen quickly when the material is exposed to elevated temperatures, thereby reducing the creep strength. To improve the creep strength of the steel, it is beneficial to decrease as much as possible the fraction of $M_{23}C_6$ and maximize the fraction of MX. However, it is also important to maintain a small martensitic grain size by controlling the prior austenite grain growth and guaranteeing a fully martensitic structure without ferrite.

By using the thermodynamic database coupled to a search algorithm described in the previous sections, a selection of compositions were filtered out based on their expected microstructure and hence their mechanical properties after Q&T treatment. The simulated T_{norm} is chosen as the highest possible temperature, taking into account the need to limit the austenite grain growth and maximizing dissolution of MX particles at T_{norm}. The optimization in terms of T_{temp} shows that there are two pathways to obtain a local optimum in terms of martensitic structure with fine MX precipitates after tempering (Table 3). The first pathway, at T_{temp} = 780 °C, leads to the composition having a minimum volume fraction of VN at T_{norm}. This is in fact due to the last added constraint “VN min” and resulted in the optimized composition alloy nr. 1

(Table 4 alloy nr. 1). The reason for this choice was discussed earlier (section 3.1 Thermodynamic model). However, the other pathway, at T_{temp} = 650 °C, leads to the composition with a minimum TaC fraction at T_{norm} (it should be noted that the TaC fraction is not zero at T_{norm} and, therefore, the TaC particles could still pin the austenite boundaries at T_{norm}). This composition is denoted as alloy nr. 12 (Table 4 alloy nr. 12).

Thermodynamic equilibrium calculations of MX and $M_{23}C_6$ f_{vol} in EU97-2, 0.05C_0.037N grade, model alloy nr. 1 and model alloy nr. 12 at experimental or simulated T_{norm} and T_{temp}, and at the expected in-service temperature ($T_{service}$) of 650 °C, are given in Table 7. The thermodynamic data show that, for both alloys suggested by the search algorithm, a larger fraction of MX carbonitrides and a lower fraction of $M_{23}C_6$ carbides will precipitate at T_{temp} and $T_{service}$ in comparison with EU97-2. Ideally, one should look for this tendency in an experimental grade. Table 5 shows that the compositions of 0.05C_0.037N and the model alloy nr. 12 are quite similar. However, 0.05C_0.037N has a lower Ta and N content, leading to a lower fraction of MX at T_{temp}, than the alloy nr. 12 (Table 7). Nevertheless, an improved creep resistance is expected for the experimental grade in comparison with EU97-2, based on the fine-tuning of C_C, C_V, C_{Ta} and C_N by the search algorithm, i.e., the higher concentration of V and Ta and lower concentration of C in the 0.05C_0.037N grade with respect to the composition of EU97-2.

Table 7: Thermodynamic equilibrium calculations of MX and $M_{23}C_6$ f_{vol} in EU97-2, 0.05C_0.037N grade, model alloy nr. 1 and model alloy nr. 12 at experimental or simulated T_{norm} and T_{temp} and at in-service temperature of 650 °C.

After normalizing	**EU97-2**	**0.05C_0.037N**	**Alloy nr. 1**	**Alloy nr. 12**
[°C]	**980 °C**	**1050 °C**	**1050 °C**	**1050 °C**
f_{vol} prec.	0.20%	0.16%	0.28%	0.32%
MX	0.20%	0.16%	0.28%	0.32%
TaC	22%	26%	79%	11%
VN	78%	74%	21%	89%
$M_{23}C_6$	0.0%	0.0%	0.0%	0.0%

After tempering	**EU97-2**	**0.05C_0.037N**	**Alloy nr.1**	**Alloy nr. 12**
[°C]	**760 °C**	**750 °C**	**780 °C**	**650 °C**
f_{vol} prec.	2.3%	1.0%	0.57%	0.73%
MX	0.32%	0.37%	0.55%	0.47%
TaC	17%	29%	57%	39%
VN	83%	71%	43%	61%
$M_{23}C_6$	2.0%	0.63%	0.020%	0.27%

In-service	**EU97-2**	**0.05C_0.037N**	**Alloy nr.1**	**Alloy nr. 12**
[°C]	**650 °C**	**650 °C**	**650 °C**	**650 °C**
f_{vol} prec.	2.36%	1.1%	0.67%	0.73%
MX	0.32%	0.37%	0.53%	0.47%
TaC	18%	30%	57%	39%

VN	82%	70%	43%	61%
$M_{23}C_6$	2.0%	0.69%	0.14%	0.27%

The 0.05C_0.037N grade, has been tested and characterized in order to verify that, as predicted by the model, such a composition actually provides an improved creep behaviour, as well as an overall satisfactory mechanical behaviour. Based on the LOM images, the microstructures of 0.05C_0.37N and EU97-2 appear similar and fully martensitic (Fig. 4). The performed heat treatment of 0.05C_0.037N can be compared with the Q&T that was given to EU97-2, as the T_{norm} was in both cases chosen as A_{c3} + 100 °C. The resulting martensitic structure of 0.05C_0.037N (GS = 7 μm) is slightly smaller than the microstructure of EU97-2 (GS = 10 μm), which leads to a lower (and therefor better) DBTT value with respect to EU97-2 (Table 5).

The impact data show that the upper shelf energy (USE) of 0.05C_0.037N is significantly lower than that of EU97-2. In contrast, the yield strength of the 0.05C_0.037N grade, 593 ± 2 MPa, is considerably higher than EU97-2 with a YS of 543 MPa. The ultimate tensile strength is also slightly higher. ICPMS data of 0.05C_0.037N showed that less Ta precipitated after the Q&T treatment, which is in agreement with Table 6, showing that the MX particles consist of 29 % TaC and 71 % VN. Comparison of ICPMS data for 0.05C_0.0.37N and for an EUROFER grade, showed that more W and C concentration will be precipitated after Q&T treatment in EUROFER, with 13 % and 10 % of the bulk value, respectively. Larger and more $M_{23}C_6$ carbides are therefore expected to be found in EU97-2 than in the 0.05C_0.037N grade or in either alloys suggested by the algorithm (Table 7). The larger $M_{23}C_6$ carbides exhibit less pinning effect on the grain boundaries and higher probability of creep void nucleation [26]. This is in agreement with the findings by J. Chen [23], showing a decrease in size and volume fraction of $M_{23}C_6$, with a reduction in carbon content of RAFM steels, confirming the equilibrium calculations in Table 7. Additionally, the solid solution strengthening of the 0.05C_0.037N grade will be higher. Literature also suggest that a higher solid solution strengthening caused by W and N is beneficial for creep resistance [27]. Overall, it appears that the mechanical properties of the 0.05C_0.037N grade are better compared to EU97-2. Moreover, creep test performed to determine the high temperature long term behaviour of the material showed that the 0.05C_0.037N indeed has better creep resistance compared to EU97 and EU97-2 (Fig. 7).

The experimental work therefor confirms that the search algorithm used to manipulate the thermodynamic database does suggest compositions and heat treatments with better mechanical properties. Based on the chosen constraints, the algorithm selects a microstructure with fine, homogeneously distributed MX carbonitrides after tempering that contribute to the strength. Further increase in MX fraction and reduction in $M_{23}C_6$ as indicated by the algorithm (Table 7) should further increase the strength of the alloy compared to EU97-2. Future considerations include the study of the effect of tempering temperature and tempering time on the size and spatial distribution of the precipitates in the experimental alloy 0.05C_0.037N and the production and study of the model alloys nr. 1 & 12.

5. Conclusions

This work proposes a new way of exploiting thermodynamic modelling in steel design. A search algorithm has been developed to select a combination of composition and heat treatments that leads to improved creep resistance with respect to the reference material EU97-2. This was validated by experimental work. The outlook includes the incorporation of kinetics in the database for better predictions of the normalization and tempering temperature and time, and the production of alloys according to the indications of the search algorithm. The search algorithm might also be further improved by using machine learning techniques.

Acknowledgements

This work has been carried out within the framework of the EUROfusion Consortium and has received partial funding from the Euratom research and training programme 2014-2018 under grant agreement No 633053. The authors wish to thank the technical staff of the Research Centre OCAS, Zwijnaarde, for the production of the material and the execution of the heat treatment. The views and opinions expressed herein do not necessarily reflect those of the European Commission.

References

[1] E. Diegele, (Structural) Materials for DEMO R&D Status, (2011).

[2] E. Materna-Morris, C. Adelhelm, S. Baumgärtner, B. Dafferner, P. Graf, S. Heger, U. Jäntsch, R. Lindau, C. Petersen, M. Rieth, R. Ziegler, H. Zimmerman, Structural material EUROFER97-2, Characterization of Rod and Plate Material: Structural, Tensile, Charpy and Creep Properties, Institut für Materialforschung, Forschungszentrum Karlsruhe, 2007.

[3] E. Fray, The heat treatment and microstructural optimization of a T91/ Fe12Cr2Si Steel composite for use as Piping and Fuel Cladding in the Lead-Bismuth cooled nuclear reactor, Mod. Phys. Metall. (2012) 1–18.

[4] E. Gaganidze, J. Aktaa, Assessment of neutron irradiation effects on RAFM steels, Fusion Eng. Des. 88 (2013) 118–128. doi:10.1016/j.fusengdes.2012.11.020.

[5] G. Federici, W. Biel, M.R. Gilbert, R. Kemp, N. Taylor, R. Wenninger, European DEMO design strategy and consequences for materials, Nucl. Fusion. 57 (2017). doi:10.1088/1741-4326/57/9/092002.

[6] R. Lindau, A. Möslang, M. Rieth, M. Klimiankou, E. Materna-Morris, A. Alamo, A.A.F. Tavassoli, C. Cayron, A.M. Lancha, P. Fernandez, N. Baluc, R. Schäublin, E. Diegele, G. Filacchioni, J.W. Rensman, B. v d Schaaf, E. Lucon, W. Dietz, Present development status of EUROFER and ODS-EUROFER for application in blanket concepts, Fusion Eng. Des. 75–79 (2005) 989–996. doi:http://dx.doi.org/10.1016/j.fusengdes.2005.06.186.

[7] F. Abe, M. Taneike, K. Sawada, Alloy design of creep resistant 9Cr steel using a dispersion of nano-sized carbonitrides, Int. J. Press. Vessel. Pip. 84 (2007) 3–12. doi:http://dx.doi.org/10.1016/j.ijpvp.2006.09.003.

[8] D. Rojas, J. Garcia, O. Prat, G. Sauthoff, A.R. Kaysser-Pyzalla, 9%Cr heat resistant steels: Alloy design, microstructure evolution and creep response at 650°C, Mater. Sci. Eng. A. 528 (2011) 5164–5176. doi:http://dx.doi.org/10.1016/j.msea.2011.03.037.

[9] R.O. Kaybyshev, V.N. Skorobogatykh, I.A. Shchenkova, New martensitic steels for fossil power plant: Creep resistance, Phys. Met. Metallogr. 109 (2010) 186–200.

doi:10.1134/S0031918X10020110.

[10] T. Jayakumar, M.D. Mathew, K. Laha, High temperature materials for nuclear fast fission and fusion reactors and advanced fossil power plants, Procedia Eng. 55 (2013) 259–270. doi:10.1016/j.proeng.2013.03.252.

[11] B. Sonderegger, S. Mitsche, H. Cerjak, Microstructural analysis on a creep resistant martensitic 9–12% Cr steel using the EBSD method, Mater. Sci. Eng. A. 481–482 (2008) 466–470. doi:http://dx.doi.org/10.1016/j.msea.2006.12.220.

[12] A. Puype, L. Malerba, N. De Wispelaere, R. Petrov, J. Sietsma, Effect of processing on microstructural features and mechanical properties of a reduced activation ferritic/martensitic EUROFER steel grade, J. Nucl. Mater. 494 (2017) 1–9. doi:10.1016/j.jnucmat.2017.07.001.

[13] A. Puype, L. Malerba, N. De Wispelaere, R. Petrov, J. Sietsma, Effect of W and N on mechanical properties of reduced activation ferritic/martensitic EUROFER-based steel grades, J. Nucl. Mater. 502 (2018) 282–288. doi:10.1016/j.jnucmat.2018.02.017.

[14] Thermo Calc, Thermo-Calc Documentation Set Version 2017a, 2017.

[15] Thermo-Calc, Thermo-Calc Software TCFE7, Steels/Fe-based Alloys Database, 2013. http://www.thermocalc.com/media/10306/tcfe7_extended_info_2013-02-07.pdf.

[16] A. Kohyama, A. Hishinuma, D.S. Gelles, R.L. Klueh, W. Dietz, K. Ehrlich, Low-activation ferritic and martensitic steels for fusion application, J. Nucl. Mater. 233–237 (1996) 138–147. doi:10.1016/S0022-3115(96)00327-3.

[17] S.L. Dudarev, J.L. Boutard, R. Lässer, M.J. Caturla, P.M. Derlet, M. Fivel, C.C. Fu, M.Y. Lavrentiev, L. Malerba, M. Mrovec, D. Nguyen-Manh, K. Nordlund, M. Perlado, R. Schäublin, H. Van Swygenhoven, D. Terentyev, J. Wallenius, D. Weygand, F. Willaime, The EU programme for modelling radiation effects in fusion reactor materials: An overview of recent advances and future goals, J. Nucl. Mater. 386–388 (2009) 1–7. doi:http://dx.doi.org/10.1016/j.jnucmat.2008.12.301.

[18] C.A. Danon, C. Servant, Thermodynamic Modeling in Reduced Activation Steels, ISIJ Int. 45 (2005) 903–912. doi:10.2355/isijinternational.45.903.

[19] C. Wang, C. Zhang, Z. Yang, J. Zhao, Multiscale Simulation of Yield Strength in Reduced-Activation Ferritic/Martensitic Steel, Nucl. Eng. Technol. 49 (2017) 569–575. doi:10.1016/j.net.2016.10.006.

[20] M. Rieth, The Chemical composition of the EUROFER steel - Historical development, overview, and critical assessment, 2007.

[21] K.S. Chandravathi, C.S. Sasmal, K. Laha, P. Parameswaran, M. Nandagopal, V.D. Vijayanand, M.D. Mathew, T. Jayakumar, E. Rajendra Kumar, Effect of isothermal heat treatment on microstructure and mechanical properties of Reduced Activation Ferritic Martensitic steel, J. Nucl. Mater. 435 (2013) 128–136. doi:http://dx.doi.org/10.1016/j.jnucmat.2012.12.042.

[22] J. Wang, S. Lu, W. Dong, D. Li, L. Rong, Microstructural evolution and mechanical properties of heat affected zones for 9Cr2WVTa steels with different carbon contents, Mater. Des. 64 (2014) 550–558. doi:10.1016/j.matdes.2014.08.018.

[23] J. Chen, C. Liu, Y. Liu, B. Yan, H. Li, Effects of tantalum content on the

microstructure and mechanical properties of low-carbon RAFM steel, J. Nucl. Mater. 479 (2016) 295–301. doi:http://dx.doi.org/10.1016/j.jnucmat.2016.07.029.

[24] R. Kirana, S. Raju, R. Mythili, S. Saibaba, T. Jayakumar, E. Rajendra Kumar, High-Temperature Phase Stability of 9Cr-W-Ta-V-C Based Reduced Activation Ferritic-Martensitic (RAFM) Steels: Effect of W and Ta Additions, Steel Res. Int. 86 (2015) 825–840. doi:10.1002/srin.201400183.

[25] N. Bernier, L. Bracke, L. Malet, S. Godet, Crystallographic reconstruction study of the effects of finish rolling temperature on the variant selection during bainite transformation in C-Mn high-strength steels, ocas Université Libre de Bruxelles [Bruxelles] (ULB), 2013. https://hal.archives-ouvertes.fr/hal-00871884.

[26] W. Yan, W. Wang, Y. Shan, K. Yang, W. Sha, 9-12Cr Heat-Resistant Steels, Springer International Publishing, 2015. https://books.google.be/books?id=0Z64CQAAQBAJ.

[27] S. Abouzari, Solid solution strengthening effect on creep strength of austenitic stainless steel, (2012) 7–13.